Forschung im Ingenieurwesen (2026)90:1
https://doi.org/10.1007/s10010-025-00929-5

ORIGINALARBEITEN/ORIGINALS

Characterization of passive recirculation in polymer electrolyte membrane fuel cells in automotive application

M. Osterhammer[1,2] · S. Held[1] · F. Du[1] · N. Feldkeller[1] · V. Formanski[1] · M. Heldwein[2]

Received: 21 October 2024 / Accepted: 4 November 2025

Abstract
Fuel cell electric vehicles offer a promising alternative to battery electric vehicles and are characterized, among other things, by rapid refueling. Recirculation in the H_2 supply system is crucial for efficient and safe fuel cell system operation in automotive applications. Typically, an ejector is used for this purpose, which, among other things, recirculates unused H_2 from the fuel cell outlet to the fuel cell inlet. The ejector in the H_2 supply system uses the H_2 inflow from a high-pressure tank as a propellant. A component test bench is developed to characterize ejectors, which enables a full-factorial measurement. In addition, the four critical operating parameters are identified: Primary flow, gas composition in the secondary flow, discharge pressure, and pressure difference between secondary and discharge pressure. The results of the measurements are brought into the context of fuel cell systems so that an operating strategy can be derived for any H_2 supply system with the characterized ejector. Depending on the primary flow rate through the ejector, an optimal outlet pressure for recirculation is determined. The H_2 molar fraction in the secondary path is identified as a key parameter for recirculation in the H_2 supply system. The ejector characterization method of this contribution makes it possible to compare the recirculation capability of an ejector within different H_2 supply systems without the need for a complete fuel cell system test bench.

1 Introduction

Fuel cell (FC) electric vehicles offer a viable alternative to battery electric vehicles, excelling in fast refueling, heavy-duty applications, and cold-temperature operation [1]. The FC system within an automotive powertrain generates power by consuming H_2 at the fuel cell anode and oxygen from the air at the FC cathode. Several fuel cells can be combined to create a FC stack for higher power and voltage output [2]. A reliable hydrogen supply is key for the safe and reliable operation of the FC system [3].

Figure 1 shows a typical automotive hydrogen supply system of a FC system. A pressure control strategy ensures a stationary anode inlet pressure p_{Dis} by adapting the primary H_2 molar flow rate $\dot{n}_{\mathrm{Prim}}$ from the H_2 storage to the H_2 supply system (HSS) [4]. For this pressure control, an injector valve's opening is adapted. The p_{Supply} is held at a constant value typically in the range of 10 to 20 bar, e.g., 15 bar in automotive applications [4]. With a typical HSS system pressure, p_{Dis} below 3 bars [5], the H_2 flow through the injector nozzle is choked in any given instance. In the present configuration, the backpressure can only be changed in front of the injector nozzle and not directly in front of the ejector. We can describe the isentropic choked flow with a flow constant C_{Inj}, the controllable injector opening area A_{Inj}, the universal gas constant R, the molar mass of H_2 M_{H2}, the temperature of the primary gas T_{Prim} and the isentropic coefficient γ [6].

$$\dot{n}_{\mathrm{Prim}} = C_{\mathrm{Inj}} \cdot A_{\mathrm{Inj}} \cdot \frac{p_{\mathrm{Prim}}}{\sqrt{R \cdot M_{\mathrm{H2}} \cdot T_{\mathrm{Prim}}}} \cdot \sqrt{\gamma \cdot \left(\frac{2}{\gamma+1}\right)^{(\gamma+1)/(\gamma-1)}} \tag{1}$$

Ceteris paribus, we can conclude from Eq. 1 that the flow through the injector is directly proportional to the opening area of the injector. In the FC stack, the H_2 is partly con-

A patent concerning the test bench methodology has been submitted to the German Patent and Trade Mark Office with the number 10 2024 110 178.4.
The results will also be published in context of the conference VDI-SIMVEC 2024.

✉ M. Osterhammer
martin.osterhammer@tum.de

[1] BMW Group, Petuelring 130, 80809 Munich, Germany

[2] chair of high-power converter systems, Technical University of Munich, Arcisstr. 21, 80333 Munich, Germany

Published online: 02 December 2025

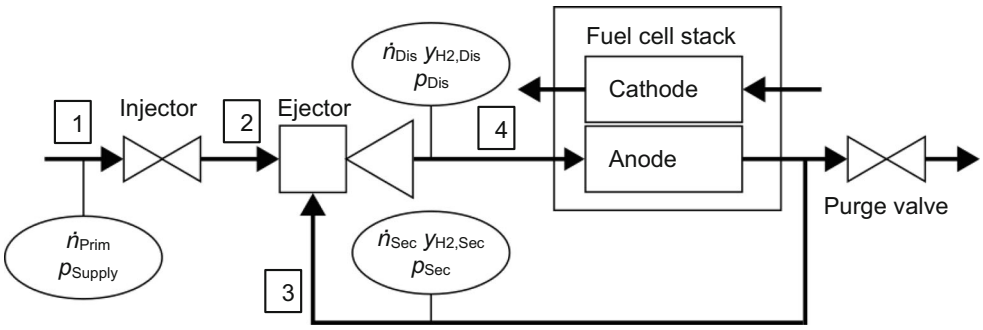

Fig. 1 Simplified H_2 supply system of a fuel cell system with passive recirculation. The ejector is the driving component for recirculation. A purge valve can be actuated to release gases to counteract a water and N_2 build-up

sumed, and N_2 can permeate from the cathode to the anode, altering the hydrogen molar fractions $y_{H2,\,Sec}$, and $y_{H2,\,Dis}$. A N_2 build-up can lead to hydrogen dilution and starvation [7]. Additionally, water crossover from cathode to anode alters the gas composition and can lead to a two-phase flow [8]. The amount of liquid water is dependent on the relative humidity and temperature [9]. A purge valve at the HSS stack outlet periodically vents gases to counteract N_2 build-up. The gas mixture at the HSS stack outlet is recirculated passively through the ejector as a secondary molar flow $\dot{n}_{Sec}$, mixed with the recirculation driving fresh H_2 feed, and discharged to the anode $\dot{n}_{Dis}$. The pressure loss $\Delta p = p_{Dis} - p_{Sec}$ over the HSS of the recirculation flow is overcome through the ejector, where the FC stack is the dominant contributor to the pressure loss. H_2 recirculation is crucial for FC system efficiency and robustness, though assessing ejector performance is complex due to the variable conditions and implicit system behavior [10]. We propose a method to characterize the ejector independently of the rest of the HSS through test bench measurements. The pressure drop characteristics of the rest of the HSS complement the ejector characterization. Suppose both HSS pressure drop and ejector characteristics are combined. In that case, the resulting point of operation of the combined system (HSS + ejector) can be determined.

Key Contributions of this research on fuel cell system ejector characterization are:

- Development of an ejector component test bench,
- Comprehensive full-factorial ejector measurements,
- Identification of four critical ejector performance parameters,
- Optimizing the discharge pressure concerning recirculation,
- Determining the H_2 recirculation in a FC system without a FC system test bench.

2 State of the art

The recirculation of the anode outlet flow to the inlet side is an essential factor in enhancing H_2 utilization. The two most prominent recirculation devices are the recirculation blower/compressor and the ejector. Where the blower is more straightforward to design and adaptable to different operating conditions, it usually has higher weight and costs. It is prone to freezing, corrosion, vibration, and noise due to its moving parts. As a passive solution without moving parts, the ejector excels with its geometric simplicity, compact design, low noise emission, and low losses with no active power consumption. However, designing and adapting an ejector is more challenging than a blower since the recirculation flow of an ejector is the result of its geometry and the FC operating parameters. Therefore, the ejector recirculation flow cannot be manipulated directly, given a fixed hardware design [11–17].

The optimal hardware design of ejectors as a single component is a well-studied subject in the literature [18–21]. However, the effective integration of ejectors within a HSS of FC systems poses several challenges. The discharge flow of the ejector influences the secondary flow and poses an implicit problem, which is hard to calculate in real-time and needs significant fitting from measurements [22, 23]. The ejector with fixed geometry is usually optimized for a limited range of operations [24]. Several methods have been developed to expand the effective range of operations. From multi-stage ejectors [25] to systems featuring adjustable ejector geometries [26], the sophistication of these systems significantly enhances their performance and adaptability. Recirculation can be quantified; furthermore, it is common practice to assess the performance of a combined FC system test bench in terms of its recirculation capabilities [27, 28], where the actual FC anode is sometimes replaced with an equivalent manifold [29]. The measurements of a combined FC system show that a certain ejector is suitable, fulfilling a specific FC system's energy efficiency [30]. An ongoing research subject is optimizing the ejector performance and, therefore, the FC system through operational strategy and determining the ejector characteristics within the FC context [31]. Thus, an in-depth design simulation, including optimization and a comprehensive test bench survey via measurement, is crucial to ensure sufficient recirculation during operation. For the durability of FC systems, the anode stoichiometry is crucial, which puts the consumed H_2 $\dot{n}_{H2,\,Consumed}$ and the fed-in hydrogen $\dot{n}_{H2,\,Dis}$ into rela-

tion $\lambda = \dot{n}_{H2,\,Dis}/\dot{n}_{H2,\,Consumed}$ [32]. The fed in H_2 equals the same amount of H_2 as the fuel cells consume for stationary pressures, disregarding purge and crossover effects [5]:

$$\dot{n}_{Prim} = \dot{n}_{H2,\,Consumed} \text{ FOR : } p_{Dis} = \text{const.} \tag{2}$$

The consumed H_2 can be determined through Faraday's Law with the FC current I_{Stack}, the number of fuel cells z and the Faraday constant F [33]. We can conclude that the operation of the FC determines the primary flow by combining Eqs. 2 and 3.

$$\dot{n}_{H2,\,Consumed} = \frac{I_{Stack} \cdot z}{2 \cdot F} \tag{3}$$

The discharged H_2 consists of the fresh H_2 from the injector and the recirculated H_2 from the secondary flow:

$$\dot{n}_{H2,\,Dis} = \dot{n}_{H2,\,Prim} + \dot{n}_{Sec} \cdot y_{H2,\,Sec} \tag{4}$$

With Eq. 4, we can express the stoichiometric ratio λ as:

$$\lambda = \frac{\dot{n}_{H2,\,Prim} + \dot{n}_{Sec} \cdot y_{H2,\,Sec}}{\dot{n}_{Prim}} \tag{5}$$

Since the primary flow is set through the operation of the FC, the stoichiometric ratio is determined through recirculation, i.e., secondary flow and its H_2 fraction.

Findings from the literature regarding the main effects on the entrainment ratio and the anode stoichiometry are collected in Table 1. The most common tools for characterization are analytical and 1D models, 2D rotational symmetric CFD models (often instead of full 3D CFD due to simulation time demands), and test bench investigations. Further information on ejectors can be found in a comprehensive literature review by Tashtoush et al. (2019) [34], Liu et al. (2020) [35] and Arabbeiki et al. (2024) [36]. Singer et al. (2022) [37] provided an extensive toolchain in an application for a pulsed ejector configuration. The literature in Table 1 clearly shows the tendency of several quantities. The findings in the literature align with the quantities of primary pressure p_{Prim} and primary Temperature T_{Prim}, which both have an increasing effect on the secondary flow. But the literature otherwise focused on different parameters like the primary mass flow $\dot{m}_{Prim}$, the gas composition $y_{H_2,\,Sec}$, the length of the mixing chamber $l_{Mixing\ Chamber}$, the humidity in the secondary flow φ_{Sec} or the discharge pressure p_{Dis}. Huang et al. (2023) state that an increased temperature in the secondary path T_{Sec} also increases the entrainment ratio. However, the other authors state the contrary. To solve this contradiction, the humidity φ, as cross-dependencies of the temperature would have to be analyzed more in-depth.

Most measurements and simulations of Table 1 include an emulated (with regards to pressure loss behavior and sometimes H_2-consumption) or an actual FC stack. The results of the ejector characterization and the specific FC stack behavior are strongly coupled. The measurements of a combined system with an ejector and FC stack cannot be easily transferred to a system with a different FC stack. Suppose the recirculation performance of different stacks combined with the same ejector is evaluated. Regarding recirculation, one must conduct a system test or simulation

Table 1 Effects of ejector design and operation conditions on recirculation and stoichiometry—examples from the literature.

Ref.	Simulation type	Measurement type	Validation	Optimization/findings	Application/ Stack power
Huang 2023 [46]	Rot.sym; CFD	$\dot{m}_{Prim}$-var. with PEMFC model	3D-printed prototype	$T_{Sec} \uparrow\rightarrow \lambda \uparrow$ $T_{Sec} \uparrow\rightarrow \omega \uparrow$ $p_{Prim} \uparrow\rightarrow \omega \downarrow$ $p_{Prim} \uparrow\rightarrow \lambda \downarrow$	PEMFC 10 kW
Singer 2023, Singer 2024 [13, 40]	Rot.sym. 2D CFD (part of design toolchain) + LHS DoE ($\mathcal{D}^{7/10} \rightarrow \mathcal{O}^1$)	–	3D CFD + measurement	$l_{Mixing\ Chamber} \uparrow\rightarrow \omega \downarrow$ $T_{Prim} \uparrow\rightarrow \omega \uparrow$ $T_{Sec} \uparrow\rightarrow \omega \downarrow$ $y_{N2,\,Sec}$, $y_{H2O,\,Sec} \uparrow\rightarrow \omega \uparrow, \lambda \downarrow$ $y_{H_2,reci} \uparrow\rightarrow \lambda \uparrow$ $\dot{m}_{Prim} \uparrow\rightarrow \omega \uparrow$	PEMFC >30 kW
Kuo 2021 [14]	0D Matlab/ Simulink model incl. FC stack	p_{Prim}-var. in [38]	Measurement	$T_{Prim} \uparrow\rightarrow \omega \uparrow$ $p_{Prim} \uparrow\rightarrow \omega \downarrow$ $T_{Sec} \uparrow\rightarrow \omega \downarrow$ $p_{Sec} \uparrow\rightarrow \omega \uparrow$	PEMFC 80 kW
Yang 2020 [15]	Rot.sym. 2D CFD + modeled Δp ($\mathcal{D}^6 \rightarrow \mathcal{O}^1$)	Test bench (N_2 operated) + emulated stack	3 load points	$T_{Sec} \uparrow\rightarrow \lambda \downarrow$ $\varphi_{Sec} \uparrow\rightarrow \lambda \downarrow$ $p_{Dis} \uparrow\rightarrow$ $\rightarrow (p_{Sec}, p_{Nozzle}) \uparrow\rightarrow \omega \uparrow$	PEMFC 100 kW

for every single component combination using the methods of Table 1. Concerning change management, this can cause significant costs and delays in development [39]. We propose a method to determine the recirculation in a complete FC system without requiring a combined test bench. To demonstrate the test bench method, we use a given ejector prototype design for passenger vehicle applications. This design combines the injector valve and the ejector into one component. Our method includes characterizing the ejector full-factorial and combining these measurements with the pressure loss characteristics of the rest of the HSS, particularly the FC stack.

3 Method

For the proposed ejector characterization, we define a system boundary around the ejector and set the relevant boundary conditions externally through a test bench according to expected fuel cell system conditions. This testbench configuration is similar to the one introduced by Singer et al. (2024), where selected points are utilized to verify CFD simulations [40]. We increased the potential of this configuration and developed a novel method by establishing a full factorial measurement of the ejector independently from the FC system. We showcase how to reintroduce the FC system characteristics into the ejector measurements a-posteriori to derive full FC system characteristics. Thus, this method allows the transfer of the ejector performance characteristics to arbitrary FC system characteristics without additional measurements. The ejector we tested is a prototype ejector designed for typical passenger automotive FC applications, as the hydrogen project from the BMW Group with its high power and dynamic requirements [41]. The ejector prototype has extended straight drilling in the ejector nozzle compared to its nozzle diameter, enabling a Fanno Flow regime for sonic operation [42]. In the present ejector configuration, it is only possible to set a supply pressure in front of the injector valve and not directly in front of the ejector. Even though the supply pressure directly in front of the ejector and after the injector is seen as an essential parameter, we do not include it in our DOE due to a lack of measurement possibility in the integrated injector/ejector design. We keep the pressure in front of the injector at a constant level, in which the injector flow is choked. We expect dynamic gas adaptation between the injector and ejector and do not assume that the ejector flow is choked. With a Fanno flow regime, the velocity of the fresh hydrogen accelerates towards the speed of sound within the ejector for a wide range of operations. With an increase in mass flow and a velocity in the range of the speed of sound, the momentum increases with the injector opening. We suspect this to be one reason for the hardware supplier to include distinctive straight drilling within the ejector in contrast to the usually used converged or convergend-divergend nozzles as in [37]. We adopted the primary flow $\dot{n}_{\mathrm{Prim}}$ by changing the opening of the injector valve with the constant supply pressure, as it is done during operation in a combined system. The secondary flow in this test bench configuration consists of N_2 and H_2 only, even though the gases are often fully saturated with H_2O in a combined system with FCs [43]. The effect of gaseous water on the average molar mass is replicated with N_2 [40]. The effect of liquid water is neglected in the scope of this work due to hardware restrictions (currently no reliable liquid water source with adjustable droplet distribution available) and will be subject to further research. The secondary N_2 flow and the H_2 flow are individually supplied through mass flow controllers, which add up to the combined secondary flow $\dot{n}_{\mathrm{Sec}}$ with a settable H_2 fraction. We included an H_2 sensor in the secondary path to ensure the H_2 fraction. Figure 2 illustrates the schematic of the ejector component test bench, facilitating stationary measurements. The four boundary conditions of gas composition in the secondary path $y_{\mathrm{H2,\,Sec}}$, the relative injector opening $\dot{n}_{\mathrm{Prim}}/\dot{n}_{\mathrm{Prim,\,Max}}$, the discharge pressure p_{Dis}, and pressure difference $\Delta p = p_{\mathrm{Dis}} - p_{\mathrm{Sec}}$ are of significant influence on the ejector performance. We use molar quantities for their wide application in the operational strategy of FC systems [44]. The quantities in bold in Fig. 2 (p_{Supply}, $\dot{n}_{\mathrm{Sec}}$, $y_{\mathrm{H2,\,Sec}}$, p_{Dis}) are set through the test bench. The remaining quantities in Fig. 2 ($\dot{n}_{\mathrm{Prim}}$; $\dot{n}_{\mathrm{Dis}}$, $y_{\mathrm{H2,\,Dis}}$, p_{Sec}) are resulting quantities and are directly measured. Table 2 outlines the relevant parameters and the actuators used to adjust them. We employed two thermal-based Mass Flow Controllers (MFCs) with bypass systems in the secondary path for both H_2 and N_2 flow to control the H_2 fraction and the pressure difference. The secondary flow is the key variable we aim to determine. The primary mass flow is directed through the injector valve opening, while the discharge pressure is directly regulated using a diaphragm valve with a cascaded pressure control system.

The pressure sensors are oriented orthogonal to the respective flow; hence, we measure static pressure with the pressure sensors. In our test bench, we have defined the pressure difference $\Delta p = p_{\mathrm{Dis}} - p_{\mathrm{Sec}}$ and the discharge pressure p_{Dis}, and indirectly, the secondary pressure p_{Sec} as a settable quantity. In our test bench setup, however, we can only measure but not actively set the secondary pressure. Conversely, we can directly set the secondary molar flow $\dot{n}_{\mathrm{Sec}}$, which equals the recirculation in the complete FC system. However, according to our definition, the recirculation flow should be the resulting value of the measurements. To address this, we iteratively adjust the secondary flow until a defined pressure difference is achieved. The pressure difference and the secondary molar flow are complementary, assuming all other factors are equal. The adjustment pro-

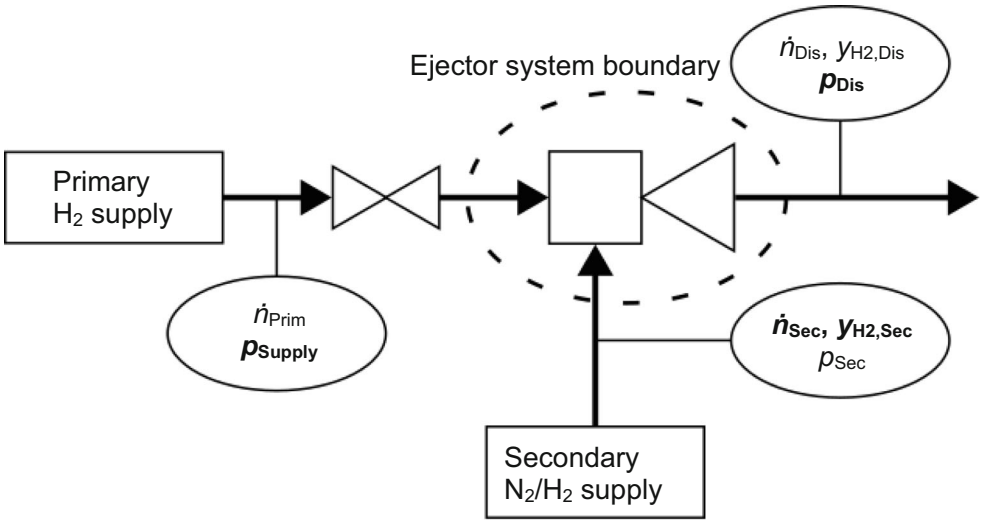

Fig. 2 Simplified test bench setup. The primary gas molar flow $\dot{n}_{Prim}$ is fed with pure H_2, while the secondary molar flow $\dot{n}_{Sec}$ is a mixture of N_2 and H_2. The parameters in bold (p_{Supply}, $\dot{n}_{Sec}$, $y_{H2,\,Sec}$, p_{Dis}) are set directly through the test bench. The remaining ($\dot{n}_{Prim}$, $\dot{n}_{Dis}$, $y_{H2,\,Dis}$, p_{Sec}) are resulting values and are measured

Table 2 List of relevant actuators for the ejector test bench, including their actuation principles. The Mass Flow Controllers (MFCs) and pressure control systems utilize cascaded feedback to maintain settable flow and pressure.

Parameter	Actuator	Actuation Principle
$\dot{n}_{Prim}$	Injector Valve	Manual Valve Control
$y_{H2,\,Sec}$	Secondary MFC N_2 and H_2	Mixing of N_2 and H_2 Flow
p_{Dis}	Diaphragm Control Valve	Directly/Cascaded Pressure Control
$\Delta p = p_{Dis} - p_{Sec}$	Secondary MFC	Directly/Cascaded Flow Control
$\dot{n}_{Sec}$	Secondary MFC	Resulting Quantity

cess took several seconds, with a sampling rate of 10 ms, resulting in a continuous variation in the pressure difference during the adaptation of the secondary flow. For data analysis in this study, we divided the measurements into increments of 5 kPa. A similar process of iterative variation is implemented for the primary molar flow $\dot{n}_{Prim}$, where the injector valve opening is adjusted at a constant supply pressure p_{Supply} until the target primary flow is reached. It is important to note that the primary molar flow $\dot{n}_{Prim}$ and the discharge pressure p_{Dis} are independent parameters at the given automotive application: Since the supply pressure p_{Supply} is multiple times higher than the discharge pressure p_{Dis}, the flow through the injector $\dot{n}_{Prim}$ is choked and hence independent on the downstream pressure p_{Dis} [37]. The discharge pressure can be reliably set through a membrane valve at the discharge path. All quantities are directly measured: $\dot{n}_{Prim}$ and $\dot{n}_{Sec}$ through mass flow sensors, $y_{H2,\,Sec}$ through an H_2 fraction sensor, and p_{Dis} and p_{Sec} with pressure sensors. We use normalized values for both flows $\dot{n}_{Sec}$ and $\dot{n}_{Prim}$, because this work focuses on establishing an ejector measurement method and the tested ejector is proprietary. Hence, we present normalized performance results. We normed the secondary molar flow $\dot{n}_{Sec,\,Norm}$ with a constant reference molar flow $\dot{n}_{Sec,Ref}$. The reference molar flow $\dot{n}_{Sec,\,Ref}$ is chosen arbitrarily, so we define $\dot{n}_{Sec,\,Norm}$ as:

$$\dot{n}_{Sec,\,Norm} = \frac{\dot{n}_{Sec}}{\dot{n}_{Sec,\,Ref}} \tag{6}$$

For the primary flow, we used a similar approach. However, we can determine a maximum primary flow, which we use as a reference value. This maximum primary flow is reached at a full injector valve opening. We use a quotient between the actual molar flow $\dot{n}_{Prim}$ to the constant maximum molar flow $\dot{n}_{Prim,\,Max}$, which equates to the relative injector opening.

$$\dot{n}_{Prim,\,Norm} = \frac{\dot{n}_{Prim}}{\dot{n}_{Prim,Max}} \tag{7}$$

Since the flow through the injector is choked in Eq. 1, we interpret the ratio in Eq. 7 as a relative injector opening.

Table 3 outlines the Design of Experiment (DoE), including the four quantities that reflect the typical operating range of an ejector in an automotive FC application. An external supplier designed the ejector hardware for the usual operational range of the automotive FC application. Where the operational range of the hydrogen fraction $y_{H2,\,Sec}$ is based on physical boundaries, the other quantities are derived through typical requirements of the fuel cells in automotive applications. We did not include a primary flow of

Table 3 Ejector test bench DoE. The range of parameters incorporates the operational range of an FC system in automotive applications.

Parameter	Range	Steps (Step Size)
$y_{H2,\,Sec}$	[0, 100] %	5 (25%)
$\dot{n}_{Prim}/\dot{n}_{Prim,\,Max}$	[11, 100] %	9 (11%)
p_{Dis}	[1, 2.5] bara	4 (0.5 bara)
$\Delta p = p_{Dis} - p_{Sec}$	[0, 30] kPa	7 (5 kPa)

zero since we do not expect any secondary flow. A discharge pressure below ambient pressure is not within a realistic use case in automotive applications since the purge process relies on overpressure. We set the pressure drop range similar to Zhang et al. [45]. Since the parameters in Table 2 depend on each other in the complete system configuration, not all combinations of values in Table 3 may be feasible in an actual FC system. However, we have created a comprehensive set of measurement points for the ejector component to interpolate from, independent of the other components in the HSS. This enables us to derive an operating strategy for any given HSS for the characterized ejector component. To predict the ejector performance in the complete system, we can complement the measurements presented here with the pressure loss characteristic of the rest of the HSS without measurements of the full system. This complementation of the pressure loss characteristic creates the dependency of the discharge quantities on the secondary quantities in the recirculation path. The adaption of changes to an HSS with a given ejector can be evaluated without extensive testing with this method at any given instance.

4 Results

Table 4 shows the qualitative test bench results, dependent on the test bench DoE of Table 3. The secondary molar flow increases with the H_2 molar fraction in the recirculation path due to the gas mixture's change in density and viscosity, which aligns well with findings from the literature [13, 14, 46, 47]. We found that a higher primary molar flow increases the secondary molar flow since the impulse input to the ejector is higher. Ejectors can have varying efficiencies at different operation points, comparing isentropic and actual enthalpy drops [48]. After surpassing an optimal injector opening, the efficiency of the ejector drops significantly since the recirculation stagnates in Fig. 6, even though the momentum of the primary flow increases [28]. To some extent, the discharge pressure influences the secondary molar flow due to the change in gas density. Therefore, adapting the stack pressure to the primary flow can increase the ejector efficiency by shifting the operating point of the ejector towards an ideally adapted nozzle [49]. We complement the literature findings by analyzing the impact of discharge pressure on secondary molar flow. We found a discharge pressure optimum for every injector opening. A deviation from this pressure decreases the secondary molar flow. In the same instance, we found a critical injector opening, after which the secondary flow stagnates or even decreases with increasing primary flow, which is in line with the findings of Pei et al. (2019) [50]. This critical injector opening is dependent on the discharge pressure. Our measurement equipment shows an uncertainty from 1% up to 3%. It is important to note that we calculate the pressure difference by subtracting two pressure sensors, thus increasing the uncertainty significantly.

Table 4 Findings on the impact of an increase in design parameters on secondary molar flow $\dot{n}_{Sec}$. The primary flow $\dot{n}_{Prim}$ and the discharge pressure p_{Dis} have a mutually dependent secondary molar flow optimum.

Parameter impact on secondary molar flow $\dot{n}_{Sec}$
$y_{H2,\,Sec} \uparrow \rightarrow \dot{n}_{Sec} \uparrow$
$\dot{n}_{Prim} \uparrow \rightarrow \begin{cases} \rightarrow \dot{n}_{Sec} \uparrow \text{ for: } \dot{n}_{Prim} < \dot{n}_{Prim,\,Crit}\,(p_{Disch}) \\ \rightarrow \dot{n}_{Sec} \searrow / \rightarrow \text{ for: } \dot{n}_{Prim} > \dot{n}_{Prim,\,Crit}\,(p_{Disch}) \end{cases}$
$p_{Dis} \uparrow \rightarrow \begin{cases} \rightarrow \dot{n}_{Sec} \uparrow \text{ for: } p_{Dis} < p_{Dis,\,Opt}\,(\dot{n}_{Prim}) \\ \rightarrow \dot{n}_{Sec} \downarrow \text{ for: } p_{Dis} > p_{Dis,\,Opt}\,(\dot{n}_{Prim}) \end{cases}$
$\Delta p \uparrow \rightarrow \dot{n}_{Sec} \downarrow$

Figure 3 shows that the pressure difference $\Delta p = p_{Dis} - p_{Sec}$ significantly decreases the recirculation flow within points of operation at 2.5 bara discharge pressure and 50% H_2 molar fraction in the secondary gas. The pressure difference can be regarded as a counteracting force to the recirculation. The curve at $\Delta p = 0$ kPa is the theoretical maximum recirculation flow within an ejector-driven system with no pressure losses. The pressure difference and the relative injector opening are set independently, meaning there could be measurements where the recirculation would be inversed. These points of inverse recirculation are impossible to depict with the test bench setup of Fig. 2, so they are measured as a flow of zero instead. Figure 3 shows the minimal injector opening for which a defined pressure drop can be achieved. A secondary flow for a pressure drop of Δp = 30 kPa is is only achievable for a relative injector opening of over 67%. The difference in relative recirculation flow depending on the pressure difference Δp decreases with a higher relative injector opening, which also corresponds to findings in the literature [14]. The curves in Fig. 3 flatten with a higher relative injector opening, hinting at the dominance of the reduced ejector efficiency.

Figure 3 shows a relation between the pressure loss Δp to the secondary molar flow $\dot{n}_{Sec}$, i.e. $\dot{n}_{Sec} = f(\Delta p)$. In the

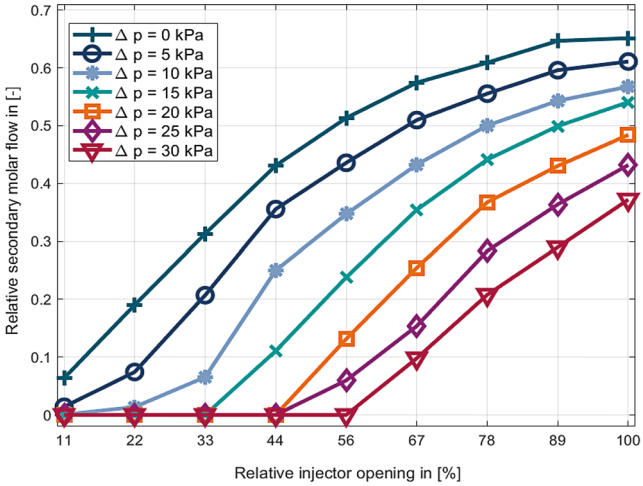

Fig. 3 The relative secondary molar flow $\dot{n}_{Sec,\,Norm}$ over the relative injector opening at different pressure differences at a discharge pressure of $p_{Dis} = 2.5$ bara and a H_2 molar fraction $y_{H2,\,Sec}$ of 50 Vol.% in the secondary flow

complete system, the pressure loss from the discharge to the secondary path results from the secondary molar flow through the HSS, where the pressure loss over the FC stack dominates. If combined with the pressure loss characteristic of the HSS, in the form of $\Delta p = f(\dot{n}_{Sec,\,Norm})$, we can derive the point of operation of the full HSS. As Fig. 4 shows, the combination of the pressure loss characteristic with the ejector characteristic can be solved graphically for a given relative injector opening. Figure 4 shows two exemplary HSS with a generic pressure loss characteristic to $\Delta p = 10\,kPa \cdot \dot{n}_{Sec,\,Norm}$ for HSS 1 as a straight line, and $\Delta p = 15\,kPa \cdot \dot{n}_{Sec,\,Norm}$ for HSS 2 as a dotted line. The point of operation can be found by determining the intersection of the ejector characteristic with the respective HSS characteristic. If the hardware components of the HSS change, the respective pressure loss characteristic of the HSS changes, resulting in a different point of operation. Depending on the system configuration, this pressure loss characteristic can deviate from a linear function. The procedure of Fig. 4 can evaluate the point of operation after changes in HSS components without the need for additional full system testing. As an additional benefit, the performance of two ejectors can be compared objectively and efficiently without the need for a full FC system test bench.

Figure 5 shows that a higher H_2 molar fraction leads to a more than proportional increase in secondary flow over the injector opening. An increase of 25 percentage points from 75 Vol.% to 100 Vol.% H_2 molar fraction leads to a doubling relative molar secondary flow. In contrast, an increase from 0 Vol.% to 25 Vol.% H_2 molar fraction is insignificant. The curves of different hydrogen fractions $y_{H2,\,Sec}$ in Fig. 5 do not differ in shape but by a multiplicative factor, and the point of no secondary flow is similar, starting at 11% relative to the injector opening. The hydrogen fraction $y_{H2,\,Sec}$ manipulation through a purging strategy is well established in the literature [51, 52]. We conclude that the secondary flow can be controlled through the hydrogen fraction using a respective purge strategy. In the same instance, the stoichiometric ratio can be determined directly, given the primary and secondary flow and the hydrogen fraction in the secondary path [38]. Regarding the stoichiometric ratio control for the hydrogen supply, the purge control strategy can be utilized similarly to the secondary flow by altering the hydrogen fraction and, hence, the stoichiometric flow, as shown in Fig. 5.

Figure 6 illustrates the impact of discharge pressure on the performance of the ejector. Low discharge pressure is ideal for the secondary flow at low injector openings. We assume that the velocities of the flows within the ejector will be higher at lower discharge pressures and injector openings, leading to increased momentum and, consequently, enhanced ejector efficiency. As the substance flow through the injector remains constant, an increase in discharge pressure increases the density, reducing the velocity and momentum.

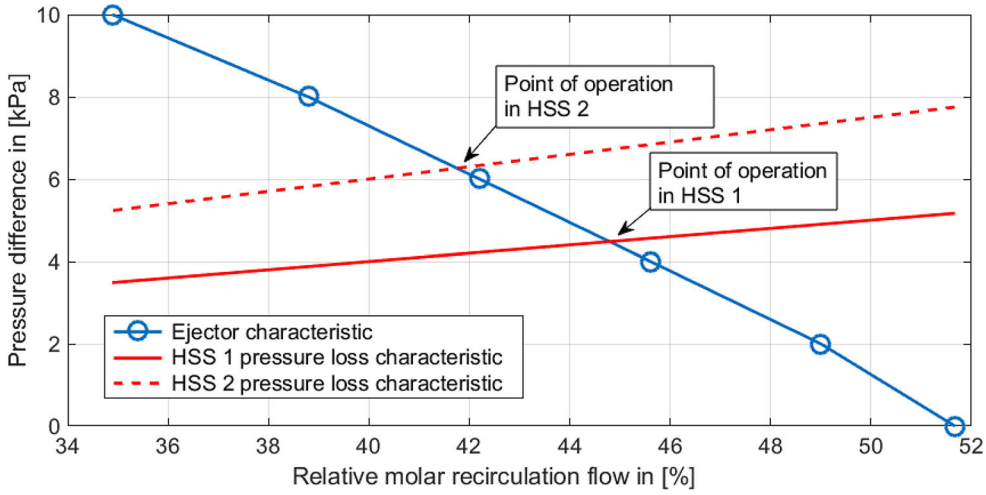

Fig. 4 The pressure difference over relative secondary molar flow $\dot{n}_{Sec,\,Norm}$ for two exemplary HSS pressure loss characteristics and the ejector characteristic at a relative injector opening of $\dot{n}_{Prim,\,Norm} = 56\%$, at a discharge pressure of $p_{Dis} = 2.5$ bara and a H_2 molar fraction $y_{H2,\,Sec}$ of 50 Vol.% in the secondary flow. The crossing of the characteristics gives the resulting point of operation

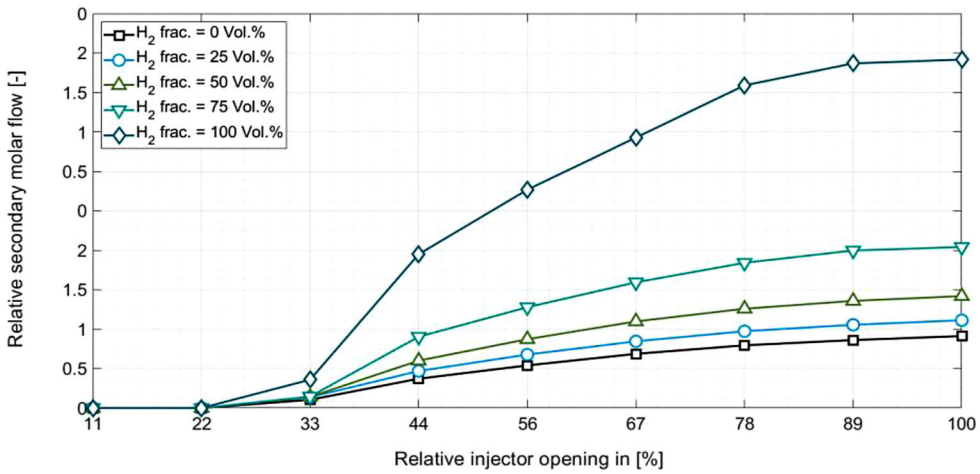

Fig. 5 The relative secondary molar flow $\dot{n}_{Sec,\,Norm}$ at a pressure difference of $\Delta p = 10\,kPa$ and a discharge pressure p_{Dis} of 2.5 bara. The higher the H_2 fraction $y_{H2,\,Sec}$, the higher the secondary molar flow $\dot{n}_{Sec}$

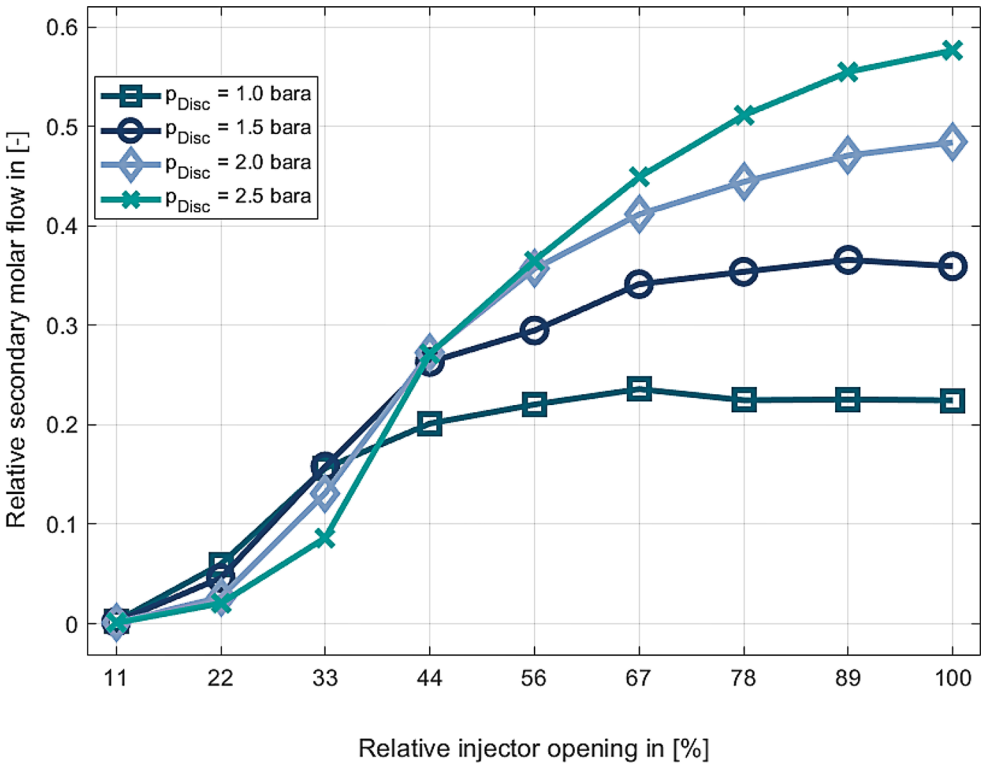

Fig. 6 The relative secondary molar flow $\dot{n}_{Sec,\,Norm}$ at a pressure difference of $\Delta p = 10\,kPa$ and $y_{H2,\,Sec} = 50\%$. The secondary flow flattens or decreases slightly for higher injector openings after a critical discharge pressure

At higher injector openings, however, there is no significant increase in the secondary flow; instead, we observe a leveling off and even a slight reduction in secondary flow. With an increase in discharge pressure, the point at which flattening occurs shifts to higher injector openings. This behavior suggests the presence of a choking effect in the secondary path. An increase in discharge pressure, maintained at a constant pressure difference, raises the pressure in the secondary path, increasing the density of the secondary flow and a subsequent decrease in velocity for the same flow rate. Consequently, the critical speed of sound is reached at higher flow rates when discharge pressures are increased.

Figure 7 illustrates the optimization of secondary flow concerning the discharge pressure based on Fig. 6. The optimal discharge pressure varies significantly for different injector openings, as the secondary flow reaches its peak when the primary gas flow through the ejector is ideally matched. We have assessed only four discharge pressure levels, with relatively large increments of 0.5 bar. Therefore, the assumed linearity depicted in Fig. 7 could be misleading. A finer DoE grid would be necessary to validate this linearity.

The optimal discharge pressure for injector openings below 22% and above 56% lies at the boundaries of the pressure range. As the relative injector opening varies be-

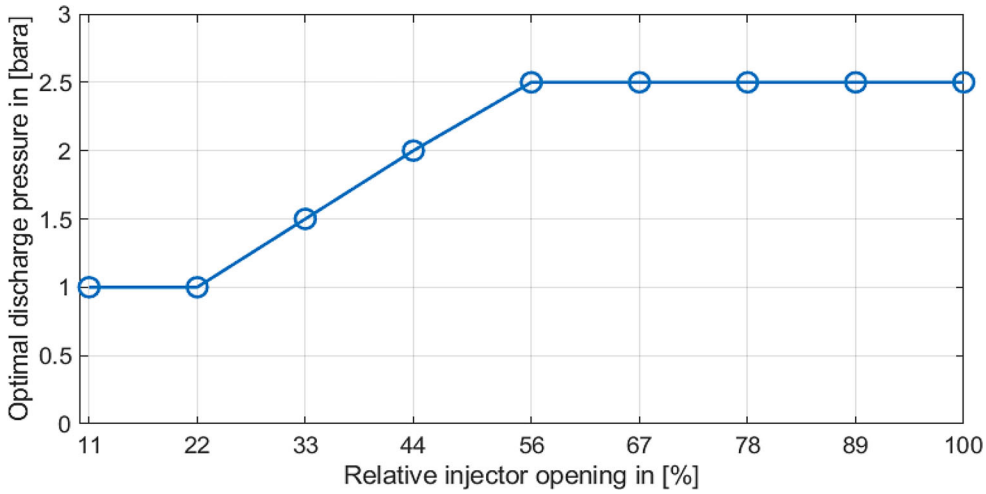

Fig. 7 Optimal discharge pressure depending on the relative injector opening of the injector. The measurements were conducted from $p_{Dis} = 1$ bara to $p_{Dis} = 2.5$ bara in steps of 0.5 bara. The points on 11% and 22% hit the lower boundary, and the points from 56% upwards hit the upper boundary pressure

tween 22% and 56%, the pressure consistently increases to achieve optimal secondary flow. Theoretically, the optimal discharge pressure is expected to continue rising beyond 2.5 bara, which may further enhance secondary flow at higher injector openings. However, our test bench and typical HSS are not designed for such high pressures.

In contrast, a decrease in pressure at 11% relative to the injector opening suggests improved secondary flow, indicating that the optimal operation of the HSS may be at a pressure below ambient levels, which is not feasible for this application. The impact of discharge pressure on secondary flow demonstrated considerable variability.

Based on the findings in Fig. 7, we can derive an optimal operational strategy for discharge pressure related to secondary flow. When considering discharge pressure and, consequently, the anode pressure operation level, a control target strategy must consider not only the optimal secondary flow but also factors concerning the longevity and safety of the FC stack.

5 Conclusion

A method for characterizing an ejector as a system component for sustainable automotive mobility was developed. This work completes findings in the literature of ejector characterization by enabling thorough validation at the test bench and the identification of the optimal discharge pressure depending on the primary mass flow. The methodology of this paper enables the determination of the secondary flow by combining the ejector component characterization and a pressure loss characteristic of the HSS. Using this methodology, operational strategies for the HSS can be derived, and changes in the system hardware can be evaluated regarding the secondary flow. The H_2 molar fraction in the secondary path is identified as a significant parameter to control the hydrogen supply's secondary flow and stoichiometric ratio.

The test bench measurements can be extended by introducing further parameters like humidity, primary and secondary flow temperature, and supply pressure. A differential pressure sensor will be integrated for future measurements, directly measuring the pressure difference from the secondary to the discharge path, decreasing measurement uncertainty. In future research, the test bench measurements can create a data-based model of the ejector, allowing for an objective and efficient comparison of the ejectors' performance.

Acknowledgements The authors deeply thank Konstantin Heidacher from BMW Group, as well as Dr. Katarzyna Kulp from the company ET EnergieTechnologie, for the competent test bench installation, qualification, support, and scrupulously carrying out the test bench measurement. We also thank Shengtao Cheng and Jakob Woelfel for improving the visualization of the measuring data.

Funding The research was funded by the BMW Group.

Funding Open Access funding enabled and organized by Projekt DEAL.

References

1. Trattner A, Klell M, Radner F (2022) Sustainable hydrogen society—vision, findings and development of a hydrogen economy using the example of Austria. Int J Hydrog Energy 47(4):2059–2079. https://doi.org/10.1016/j.ijhydene.2021.10.166
2. Qiu D, Peng L, Yi P, Lehnert W, Lai X (2021) Review on proton exchange membrane fuel cell stack assembly: quality evaluation, assembly method, contact behavior and process design. Renew Sustain Energy Rev 152:111660. https://doi.org/10.1016/j.rser.2021.111660
3. Arora D, Bonnet C, Mukherjee M, Raël S, Lapicque F (2019) Direct hybridization of PEMFC and supercapacitors: effect of excess hydrogen on a single cell fuel cell durability and its feasibility on fuel cell stack. Electrochim Acta 310:213–220. https://doi.org/10.1016/j.electacta.2019.04.073
4. Zhu Y, Zou J, Peng C, Xie Y, Li L (2017) Modelling and fuel flow control of PEMFC considering over-pressure case. In: 2017 Chinese automation congress (CAC). IEEE, Jinan, pp 2222–2225 https://doi.org/10.1109/CAC.2017.8243143
5. Li X, Wei H, Du C, Shi C, Zhang J (2023) Control strategy for the anode gas supply system in a proton exchange membrane fuel cell system. Energy Rep 10:4342–4358. https://doi.org/10.1016/j.egyr.2023.10.079
6. Lijo V, Kim HD, Setoguchi T (2010) Analysis of choked viscous flows through a constant area duct. Proc Inst Mech Eng Part G J Aerosp Eng 224(11):1151–1162. https://doi.org/10.1243/09544100JAERO785
7. Ahluwalia RK, Wang X (2007) Buildup of nitrogen in direct hydrogen polymer-electrolyte fuel cell stacks. J Power Sources 171(1):63–71. https://doi.org/10.1016/j.jpowsour.2007.01.032
8. Sun W, Zhang H, Jia L, Xue H (2022) Study on multicomponent and multiphase of the ejector for proton exchange membrane fuel cell hydrogen recirculation. J Therm Anal Calorim 147(23):13681–13697. https://doi.org/10.1007/s10973-022-11548-5
9. Yousfi-Steiner N, Moçotéguy P, Candusso D, Hissel D, Hernandez A, Aslanides A (2008) A review on PEM voltage degradation associated with water management: impacts, influent factors and characterization. J Power Sources 183(1):260–274. https://doi.org/10.1016/j.jpowsour.2008.04.037
10. Xia Z, Wang B, Yang Z, Wu K, Du Q, Jiao K (2019) Effect of operating conditions on performance of proton exchange membrane fuel cell with anode recirculation. Energy Procedia 158:1829–1834. https://doi.org/10.1016/j.egypro.2019.01.428
11. Han J, Feng J, Chen P, Liu Y, Peng X (2022) A review of key components of hydrogen recirculation subsystem for fuel cell vehicles. Energy Convers Manag X 15:100265. https://doi.org/10.1016/j.ecmx.2022.100265
12. Hou J, Yang M, Zhang J (2020) Active and passive fuel recirculation for solid oxide and proton exchange membrane fuel cells. Renew Energy 155:1355–1371. https://doi.org/10.1016/j.renene.2020.04.002
13. Singer G, Köll R, Pertl P, Trattner A (2023) Development of an ejector for passive hydrogen recirculation in PEM fuel cell systems by applying 2D CFD simulation. Automot Engine Technol 8(3):211–226. https://doi.org/10.1007/s41104-023-00133-z
14. Kuo J-K, Hsieh C-Y (2021) Numerical investigation into effects of ejector geometry and operating conditions on hydrogen recirculation ratio in 80 kW PEM fuel cell system. Energy 233:121100. https://doi.org/10.1016/j.energy.2021.121100
15. Yang Y et al (2020) Numerical studies on ejector structure optimization and performance prediction based on a novel pressure drop model for proton exchange membrane fuel cell anode. Int J Hydrog Energy 45(43):23343–23352. https://doi.org/10.1016/j.ijhydene.2020.06.068
16. Dadvar M, Afshari E (2014) Analysis of design parameters in anodic recirculation system based on ejector technology for PEM fuel cells: a new approach in designing. Int J Hydrog Energy 39(23):12061–12073. https://doi.org/10.1016/j.ijhydene.2014.06.046
17. Jenssen D, Berger O, Krewer U (2017) Improved PEM fuel cell system operation with cascaded stack and ejector-based recirculation. Appl Energy 195:324–333. https://doi.org/10.1016/j.apenergy.2017.03.002
18. Braccio S, Guillou N, Le Pierrès N, Tauveron N, Phan HT (2023) Mass-flowrate-maximization thermodynamic model and simulation of supersonic real-gas ejectors used in refrigeration systems. Therm Sci Eng Prog 37:101615. https://doi.org/10.1016/j.tsep.2022.101615
19. Sadasivan S, Arumugam SKJCR, Aggarwal MC (2023) Effects of influencing factors on the performance and morphology of shock waves in ejectors: a review. Int J Mod Phys C 34(11):2350142. https://doi.org/10.1142/S0129183123501425
20. Śmierciew K, Gagan J, Butrymowicz D (2019) Application of numerical modelling for design and improvement of performance of gas ejector. Appl Therm Eng 149:85–93. https://doi.org/10.1016/j.applthermaleng.2018.12.030
21. Lu Y, Wang X, Yang G, Xu S (2024) Numerical studies on structure optimization and flow characteristics of a hydrogen recirculation ejector under multiple load conditions. Int J Hydrog Energy 92:234–246. https://doi.org/10.1016/j.ijhydene.2024.10.252
22. Antetomaso C, Irimescu A, Merola SS, Vaglieco BM, Di Micco S, Jannelli E (2024) Ejector design for PEM fuel cells and assessment of its scalability. Int J Hydrog Energy 95:1235–1241. https://doi.org/10.1016/j.ijhydene.2024.07.433
23. Zhu Y, Li Y (2009) New theoretical model for convergent nozzle ejector in the proton exchange membrane fuel cell system. J Power Sources. https://doi.org/10.1016/j.jpowsour.2009.02.014
24. Wang X, Xu S, Xing C (2019) Numerical and experimental investigation on an ejector designed for an 80 kW polymer electrolyte membrane fuel cell stack. J Power Sources 415:25–32. https://doi.org/10.1016/j.jpowsour.2019.01.039
25. Wang X, Wang L, Song Y, Deng J, Zhan Y (2021) Optimal design of two-stage ejector for subzero refrigeration system on fishing vessel. Appl Therm Eng 187:116565. https://doi.org/10.1016/j.applthermaleng.2021.116565
26. Jenssen D, Berger O, Krewer U (2017) Improved PEM fuel cell system operation with cascaded stack and ejector-based recirculation. Appl Energy 195:324–333. https://doi.org/10.1016/j.apenergy.2017.03.002
27. Yu M, Wang C, Wang L, Wang X (2024) Flow characteristics of coaxial-nozzle ejector for PEMFC hydrogen recirculation system. Appl Therm Eng 236:121541. https://doi.org/10.1016/j.applthermaleng.2023.121541
28. Nikiforow K, Koski P, Karimäki H, Ihonen J, Alopaeus V (2016) Designing a hydrogen gas ejector for 5 kW stationary PEMFC system—CFD-modeling and experimental validation. Int J Hydrog Energy 41(33):14952–14970. https://doi.org/10.1016/j.ijhydene.2016.06.122
29. Chen L, Xu K, Yang Z, Yan Z, Dong Z (2022) Optimal design and operation of dual-ejector PEMFC hydrogen supply and circulation system. Energies 15(15):5427. https://doi.org/10.3390/en15155427
30. Nikiforow K, Koski P, Ihonen J (2017) Discrete ejector control solution design, characterization, and verification in a 5 kW PEMFC system. Int J Hydrog Energy 42(26):16760–16772. https://doi.org/10.1016/j.ijhydene.2017.05.151
31. Vincenzo L, Pagh NM, Knudsen KS (2013) Ejector design and performance evaluation for recirculation of anode gas in a micro combined heat and power systems based on solid oxide fuel cell. Appl

Therm Eng 54(1):26–34. https://doi.org/10.1016/j.applthermaleng.2013.01.021
32. Hahn S, Braun J, Kemmer H, Reuss H-C (2021) Optimization of the efficiency and degradation rate of an automotive fuel cell system. Int J Hydrog Energy 46(57):29459–29477. https://doi.org/10.1016/j.ijhydene.2020.12.084
33. O'Hayre RP, Cha S-W, Colella WG, Prinz FB (2016) Fuel cell fundamentals, third edition. Wiley, Hoboken, New Jersey
34. Tashtoush BM, Al-Nimr MA, Khasawneh MA (2019) A comprehensive review of ejector design, performance, and applications. Appl Energy 240:138–172. https://doi.org/10.1016/j.apenergy.2019.01.185
35. Liu Y, Tu Z, Chan SH (2021) Applications of ejectors in proton exchange membrane fuel cells: a review. Fuel Process Technol 214:106683. https://doi.org/10.1016/j.fuproc.2020.106683
36. Arabbeiki M, Mansourkiaei M, Ferrero D, Santarelli M (2024) Ejectors in hydrogen recirculation for PEMFC-based systems: a comprehensive review of design, operation, and numerical simulations. Energies. https://doi.org/10.3390/en17194815
37. Singer G, Gappmayer G, Macherhammer M, Pertl P, Trattner A (2022) A development toolchain for a pulsed injector-ejector unit for PEM fuel cell applications. Int J Hydrog Energy 47(56):23818–23832. https://doi.org/10.1016/j.ijhydene.2022.05.177
38. Toghyani S, Afshari E, Baniasadi E (2019) A parametric comparison of three fuel recirculation system in the closed loop fuel supply system of PEM fuel cell. Int J Hydrog Energy 44(14):7518–7530. https://doi.org/10.1016/j.ijhydene.2019.01.260
39. Tavčar J, Demšar I, Duhovnik J (2018) Engineering change management maturity assessment model with lean criteria for automotive supply chain. J Eng Des 29(4-5):235–257. https://doi.org/10.1080/09544828.2018.1463513
40. Singer G, Pinsker R, Stelzer M, Aggarwal M, Pertl P, Trattner A (2024) Ejector validation in proton exchange membrane fuel cells: a comparison of turbulence models in computational fluid dynamics (CFD) with experiment. Int J Hydrog Energy 61:1405–1416. https://doi.org/10.1016/j.ijhydene.2024.02.365
41. Seidel C BMW iX5 hydrogen pilot fleet launches. https://www.press.bmwgroup.com/global/article/detail/T0408839EN/bmw-group-brings-hydrogen-cars-to-the-road:-bmw-ix5-hydrogen-pilot-fleet-launches
42. Kumar RA, Rajesh G (2016) Flow transients in un-started and started modes of vacuum ejector operation. Phys Fluids 28(5):56105. https://doi.org/10.1063/1.4948959
43. Ma T, Yang Y, Lin W, Yang Y, Jia W, Zhang J (2019) Design of a novel high-efficiency water separator for proton exchange membrane fuel cell system. Int J Hydrog Energy 44(11):5462–5469. https://doi.org/10.1016/j.ijhydene.2018.10.109
44. Najafi B, Haghighat Mamaghani A, Rinaldi F, Casalegno A (2015) Long-term performance analysis of an HT-PEM fuel cell based micro-CHP system: operational strategies. Appl Energy 147:582–592. https://doi.org/10.1016/j.apenergy.2015.03.043
45. Zhang B et al (2023) Modeling, control and analysis of a novel energy-saving oriented fuel cell anode system. Energy Convers Manag 283:116942. https://doi.org/10.1016/j.enconman.2023.116942
46. Huang P-H, Kuo J-K, Wu C-B (2023) Simulation and experimental measurements of 10-kW PEMFC passive hydrogen recovery system. Int J Hydrog Energy 48(44):16790–16801. https://doi.org/10.1016/j.ijhydene.2023.01.136
47. Wang B et al (2019) Numerical analysis of operating conditions effects on PEMFC with anode recirculation. Energy 173:844–856. https://doi.org/10.1016/j.energy.2019.02.115
48. Besagni G, Mereu R, Inzoli F, Chiesa P (2017) Application of an integrated lumped parameter-CFD approach to evaluate the ejector-driven anode recirculation in a PEM fuel cell system. Appl Therm Eng 121:628–651. https://doi.org/10.1016/j.applthermaleng.2017.04.111
49. Śmierciew K, Gagan J, Butrymowicz D (2019) Application of numerical modelling for design and improvement of performance of gas ejector. Appl Therm Eng 149:85–93. https://doi.org/10.1016/j.applthermaleng.2018.12.030
50. Pei P et al (2019) Numerical studies on wide-operating-range ejector based on anodic pressure drop characteristics in proton exchange membrane fuel cell system. Appl Energy 235:729–738. https://doi.org/10.1016/j.apenergy.2018.11.005
51. Liu Z et al (2020) Anode purge management for hydrogen utilization and stack durability improvement of PEM fuel cell systems. Appl Energy 275:115110. https://doi.org/10.1016/j.apenergy.2020.115110
52. Chen Y-S, Yang C-W, Lee J-Y (2014) Implementation and evaluation for anode purging of a fuel cell based on nitrogen concentration. Appl Energy 113:1519–1524. https://doi.org/10.1016/j.apenergy.2013.09.028